



Mn₃O₄ nanoparticles anchored on continuous carbon nanotube network as superior anodes for lithium ion batteries



Shu Luo^{a,b}, Hengcai Wu^a, Yang Wu^a, Kaili Jiang^a, Jiaping Wang^{a,*}, Shoushan Fan^{a,b}

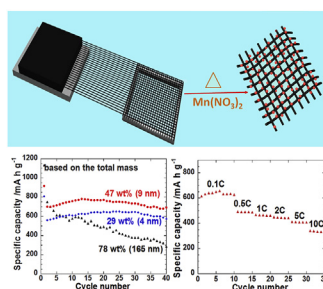
^a Department of Physics and Tsinghua-Foxconn Nanotechnology Research Center, Tsinghua University, Beijing 100084, China

^b Department of Material Science and Engineering, Tsinghua University, Beijing 100084, China

HIGHLIGHTS

- Mn₃O₄ nanoparticles are in-situ grown on continuous super-aligned CNT films.
- CNT films serve as the conductive pathway and structural scaffold in the composite.
- Binder, extra conductive agent, or current collector is not needed in the electrode.
- Sizes of the Mn₃O₄ particles are tuned to optimize the electrochemical property.
- The Mn₃O₄/CNT electrodes show stable cycle performance and high rate capability.

GRAPHICAL ABSTRACT



ARTICLE INFO

Article history:

Received 30 August 2013

Received in revised form

17 October 2013

Accepted 30 October 2013

Available online 7 November 2013

Keywords:

Manganese oxide

Carbon nanotube

Size effect

Lithium ion battery

ABSTRACT

Mn₃O₄ nanoparticles anchored on continuous super-aligned carbon nanotube (SACNT) films are synthesized by decomposition of Mn(NO₃)₂. In the Mn₃O₄/SACNT composite electrodes, SACNT film is capable of serving as both the conductive pathway and structural scaffold, therefore no binder, extra conductive agent, or current collector is needed. The electrochemical performance of the Mn₃O₄/SACNT composite electrode is significantly affected by the particle size of Mn₃O₄. With smaller particle size, the electrode displays smaller voltage hysteresis and much improved reversibility and rate capability. The Mn₃O₄/SACNT electrodes with particle size of Mn₃O₄ less than 10 nm show a capacity retention of 95% after 100 cycles at 1 C and a high rate capacity of 342 mAh g⁻¹ at 10 C (based on the total mass of the electrode), suggesting their advantages over the commercial graphite anode and potential in practical applications.

© 2013 Elsevier B.V. All rights reserved.

1. Introduction

Energy is now one of the biggest concerns all over the world, and among all the energy issues, efficient energy storage and conversion are very critical. Lithium ion battery (LIB), with its high

energy and power density and environmental friendly essence, has been considered as one of the most promising energy storage devices. Many efforts have been done to develop new electrode materials for LIBs, aiming to achieve higher capacity, longer cycle life, and better rate performance. Among all these materials, transition metal oxides have aroused tremendous interest since 2000, when Tarascon reported their potential as high capacity anodes for LIBs [1]. Unlike the intercalation compounds (such as LiCoO₂, LiMn₂O₄, graphite, TiS₂) or alloy systems (such as Sn, Sb, In, Pb, Zn, Si),

* Corresponding author. Tel.: +86 10 62796007; fax: +86 10 62792457.

E-mail address: jpwang@tsinghua.edu.cn (J. Wang).

transition metal oxides store and release Li ions through the following conversion reaction: $\text{MO}_x + 2x\text{e}^- + 2x\text{Li}^+ \rightleftharpoons \text{M}^0 + x\text{Li}_2\text{O}$ [1]. The full reduction of the transition metal oxides results in composite materials composing of metallic nanoparticles (2–8 nm) dispersed in the amorphous Li_2O matrix [2–5]. Such reaction occurs in many transition metal oxides, such as the oxides of Co, Fe, Cu, Ni, Cr, Mn, and so on [6,7]. Among them, Mn_3O_4 is non-toxic, abundant, and low-cost, with a theoretical capacity as high as 936 mAh g^{-1} , 2.5 times the capacity of the commercial graphite anode (372 mAh g^{-1}). However, there are several disadvantages of using Mn_3O_4 as anode material: 1) low conductivity (about 10^{-8} – $10^{-7} \text{ S cm}^{-1}$) [8]; 2) low coulombic efficiency (often lower than 70%); 3) large volume change (over 170%) through charge and discharge processes [9] thus leading to rapid capacity decay through cycling; and 4) poor rate performance. Pure Mn_3O_4 often demonstrated a reversible capacity of no more than 250 mAh g^{-1} [10,11]. There are two key strategies to solve these problems: 1) nanostructured Mn_3O_4 particles with no aggregation would lead to smaller reaction barrier and faster ion diffusion [12,13]. 2) Mn_3O_4 particles composited with conductive substrate or coating, such as carbon materials, would improve the electron transfer ability and prevent electrode pulverization [14,15]. By integrating these two strategies, nano- Mn_3O_4 /carbon composites displayed much improved electrochemical properties [8,16,17]. As Wang et al. showed, nano- Mn_3O_4 /graphene composite presented a high reversible capacity of 900 mAh g^{-1} and a good rate retention of 390 mAh g^{-1} at a current density of 1600 mA g^{-1} [10]. Amorphous and nanosized MnO_x (containing 70 mol% Mn_3O_4) dispersed in porous carbon spheres also displayed stable cycling performance (600 mAh g^{-1} up to 130 cycles) [18]. Most of these nano- Mn_3O_4 /carbon composites were synthesized through complicated hydrothermal method or high-temperature chemical reaction. In addition, as the carbon matrix of graphene or carbon spheres could not form a network by themselves, extra conductive agent, binder, and current collector are still needed.

In comparison with porous carbon spheres, graphene, and ordinary CNTs, super-aligned carbon nanotubes (SACNTs) are featured with large aspect ratio ($>10^4$), super-aligned structure, clean surface, and strong van der Waals force among tubes [19]. With this strong interaction, SACNT films can be successfully drawn from the SACNT arrays, forming a well-controlled and cross-stacked

network [19,20]. Due to their high conductivity, elaborate structure, and excellent mechanical properties (high strength and flexibility), SACNT films have been applied in many fields [20], including LIBs [21–24]. In this work, cross-stacked SACNT films are used to anchor Mn_3O_4 nanoparticles through the decomposition of $\text{Mn}(\text{NO}_3)_2$ infiltrated in the SACNT films. In this composite, SACNT films serve as both ordered conductive pathway and structural scaffold to anchor Mn_3O_4 nanoparticles, thus eliminating the need of binder, extra conductive agent, and current collector. Moreover, Mn_3O_4 /SACNT electrode possesses a porous structure, which would benefit the electrolyte infiltration and accommodation of the volumetric expansion during charge/discharge processes. The size of Mn_3O_4 particles is also tuned to optimize the electrochemical performance. Mn_3O_4 nanoparticles with diameter less than 10 nm anchored on cross-stacked SACNT scaffold present outstanding cycle stability and rate capability.

2. Experimental

2.1. Fabrication of the nano- Mn_3O_4 /SACNT composites

SACNT arrays with a height of $300 \mu\text{m}$ were synthesized on 4 inch silicon wafers in a low pressure chemical vapor deposition (LP-CVD) system with iron as the catalyst and acetylene as the precursor [19]. SACNT films were drawn from the SACNT arrays by an end-to-end joining mechanism [25], and cross-stacked on a $7 \text{ cm} \times 7 \text{ cm}$ aluminum frame (Fig. 1a). 100-layer cross-stacked SACNT films were soaked into the $\text{Mn}(\text{NO}_3)_2$ ethanol–water solution with different concentration of $X \text{ wt}\%$ $\text{Mn}(\text{NO}_3)_2$ (ethanol: 30 wt%, water solution: 70 wt%, X means the content of $\text{Mn}(\text{NO}_3)_2$ in water solution, $X = 3, 5, 10$). The SACNT films with infiltration of $\text{Mn}(\text{NO}_3)_2$ solution were dried and heat-treated in a furnace at $300 \text{ }^\circ\text{C}$ for 1 h in Ar to obtain the nano- Mn_3O_4 /SACNT composites.

2.2. Morphology and structure characterization

Microstructures of the Mn_3O_4 /SACNT composites were characterized using an FEI Sirion 200 scanning electron microscope (SEM) operating at 10 kV and an FEI Tecnai G2F20 transmission electron microscope (TEM) operating at 200 kV. Resistivity was measured on a Resmap 4 probe system (Creative Design Engineering Inc.,

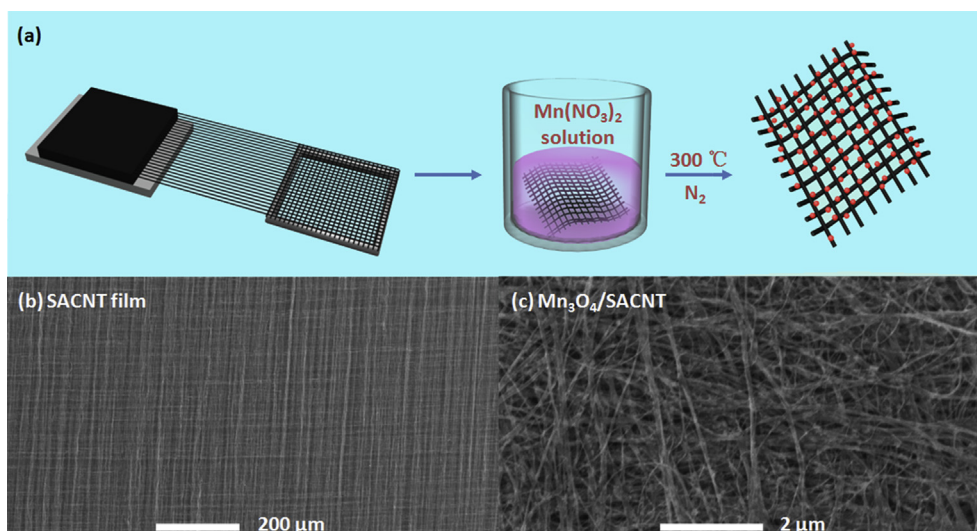


Fig. 1. a) Schematic of the fabrication of the Mn_3O_4 /SACNT composite. The right image demonstrates Mn_3O_4 nanoparticles homogeneously anchored on the cross-stacked SACNT scaffold. SEM images of the b) original 100-layer SACNT film and c) the Mn_3O_4 /SACNT composite.

USA). Powder X-ray diffraction data were collected on a Rigaku D/max 2500PC diffractometer operating at 40 kV and 200 mA with Cu $K\alpha_1$ radiation in θ – 2θ diffraction geometry. Mn_3O_4 /SACNT samples were applied on a quartz sample holder and diffraction patterns were collected in a 2θ range of 10 – 90° .

2.3. Electrochemical test

Coin-type (CR2016) half-cells were assembled in an Ar-filled glove box (M. Braun inert gas systems Co. Ltd.) with the Mn_3O_4 /SACNT composite as the positive electrode and Li metal as the negative electrode. A porous polymer film (Celgard 2400, USA) was used as the separator and 1 M $LiPF_6$ solution in ethylene carbonate (EC) and diethyl carbonate (DEC) mixed at weight ratio of 1:1 was used as electrolyte. The cells were tested using a Land battery test system (Wuhan Land Electronic Co., China) with cut-off voltages of 0.01–3 V at room temperature. Cyclic voltammetry (CV) test was conducted on a PARSTAT 2273 advanced electrochemical system in the voltage range of 0.01–3 V at a scanning rate of 0.1 mV s^{-1} .

3. Results and discussion

After decomposition of the $Mn(NO_3)_2$ infiltrated in the SACNT films, the obtained product was identified as Mn_3O_4 /SACNT composite by XRD, with a characteristic peak of CNT at 26° (Fig. 2). Other peaks were consistent with those of Mn_3O_4 phase (JCPDS 18-0803). As shown in Fig. 1b and c, the cross-stacked structure of the SACNT films was not disturbed during the formation process of Mn_3O_4 . SACNT films were composed of aligned and segregated CNTs with uniform dispersion of Mn_3O_4 nanoparticles on the intersections and walls of the CNTs, forming a porous network. By varying the concentration of the $Mn(NO_3)_2$ solution, the size of the obtained Mn_3O_4 nanoparticles can be tuned. For the 3 wt% $Mn(NO_3)_2$ solution, Mn_3O_4 particles with a diameter of 4 nm were anchored uniformly on the outer walls and intersections of the SACNTs (Fig. 3a and d), and the weight percent of Mn_3O_4 in the composite was 29 wt%. For the 5 wt% $Mn(NO_3)_2$ solution, Mn_3O_4 particles with a diameter of 9 nm were formed and densely covered the SACNT network (Fig. 3b and e). The content of Mn_3O_4 was about 47 wt%. While for the 10 wt% $Mn(NO_3)_2$ solution, Mn_3O_4 particles became much larger, with a diameter of 165 nm in average (Fig. 3c and f). These large particles were composed of small clusters (about 20 nm size) that agglomerated tightly together, counting for 78 wt% of the whole composite. The large size of the agglomerated Mn_3O_4

particles would result in reduced contact area with the conductive SACNT network and inefficient electron transfer during the cycling processes.

In spite of the insulating Mn_3O_4 particles anchored on the SACNT films, the sheet resistance of the 29 wt%, 47 wt%, and 78 wt% Mn_3O_4 /SACNT composites remained as low as 16–20 Ω per sq, which is close to 11 Ω per sq for the pristine SACNT film. The low sheet resistance of the Mn_3O_4 /SACNT composite indicated that the SACNT film in the composite still maintained its intact network structure and excellent conducting ability. Therefore, it is feasible to apply the SACNT film as the conducting network and current collector. Besides, no binder is needed, as the Mn_3O_4 nanoparticles were anchored on the SACNT film as a structure scaffold.

With different contents and sizes of Mn_3O_4 , the electrochemical performances of the Mn_3O_4 /SACNT composites were very distinct. As shown in Fig. 4a, the capacity of the 78 wt% Mn_3O_4 /SACNT decayed rapidly. After 40 cycles, it decreased to only 367 mAh g^{-1} (based on the mass of Mn_3O_4), which was 39% of the capacity at the first cycle. Considering the large agglomerated Mn_3O_4 particles with a size of 165 nm in the composite, large reaction barrier would exist and electron transfer would not be efficient, thus resulting in rapid capacity decay. When the size of the Mn_3O_4 particles was limited to less than 10 nm, the composites displayed much improved cycling stability. For the 47 wt% and 29 wt% Mn_3O_4 /SACNT composites with sizes of Mn_3O_4 at 9 nm and 4 nm, their capacities after 40 cycles remained almost the same compared with the values at the first cycle.

It is noticeable that the 47 wt% and 29 wt% Mn_3O_4 /SACNT composites displayed reversible capacity of 1502 mAh g^{-1} and 1912.9 mAh g^{-1} based on the mass of Mn_3O_4 , much higher than the theoretical values of Mn_3O_4 (936 mAh g^{-1}). Such high capacity values also led to high capacities based on the total mass of the electrode (including the weights of both Mn_3O_4 and SACNT), being 701.4 mAh g^{-1} for the 47 wt% Mn_3O_4 /SACNT composite and 560.5 mAh g^{-1} for the 29 wt% Mn_3O_4 /SACNT composite (Fig. 4b). These values are 89.3% and 50.7% higher than that of graphite, respectively. The capacities of Mn_3O_4 in the 47 wt% and 29 wt% Mn_3O_4 /SACNT composites (1502 mAh g^{-1} and 1912.9 mAh g^{-1}) are higher than its theoretical value, which is quite common for nanostructured transition metal oxides [6,23,26]. The excessive capacity could be caused by an interfacial charging mechanism where excess lithium is accommodated at the metal/ Li_2O interface [27], or the formation of a polymer/gel-like film coating on the surface of nanoparticles resulted from decomposition of the electrolyte [28]. It should be noted that the 29 wt% Mn_3O_4 /SACNT electrode contained Mn_3O_4 particles with a diameter of 4 nm, while the 47 wt% Mn_3O_4 /SACNT electrode contained Mn_3O_4 particles with a diameter of 9 nm. According to the above-mentioned mechanism, the larger specific surface area in the 29 wt% Mn_3O_4 /SACNT electrode would display higher excessive capacity than the 47 wt% Mn_3O_4 /SACNT electrode, which agrees well with the experimental data in Fig. 4a. Another possible source of the excessive capacity in the Mn_3O_4 /SACNT electrodes could be the contribution of CNTs. As the graphene layers in CNTs are closed with limited lithium insertion ability, pure CNTs performed unsatisfactorily as an anode material [29]. Many researches proved that introducing defects onto the CNT walls would improve its ability of storing Li ions [30]. To identify the contribution of the SACNT films in the composite electrode, Mn_3O_4 nanoparticles on the SACNT film were dissolved by concentrated hydrochloric acid, which would not destroy the structure of the CNT film [31]. The cycling performance of such treated SACNT film is shown in Fig. 5a. The specific capacity of CNTs gradually decreased and then stabilized around 242 mAh g^{-1} . By subtracting the capacity contribution from the SACNT film, the real capacity of Mn_3O_4 in the 47 wt% and 29 wt% Mn_3O_4 /SACNT

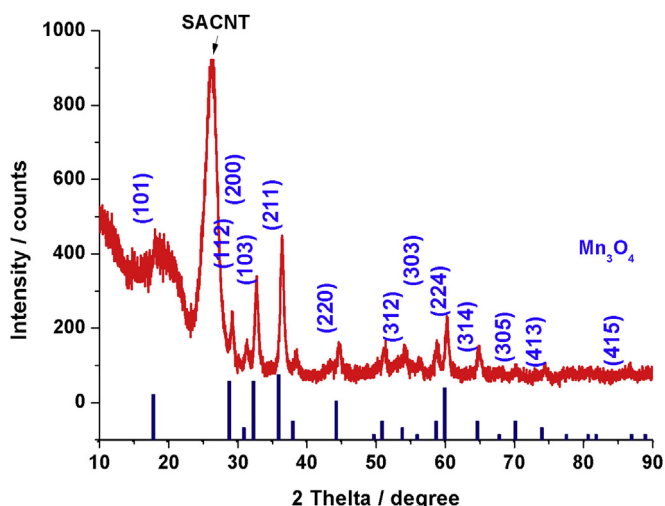


Fig. 2. XRD result of the Mn_3O_4 /SACNT composite.

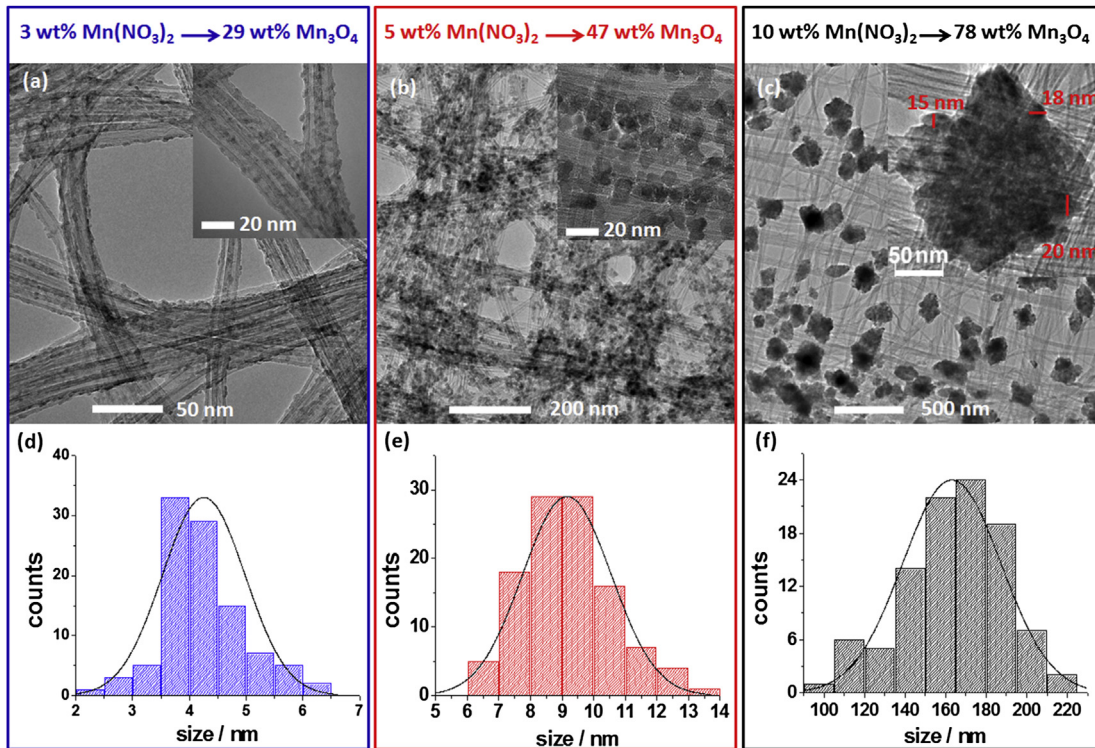


Fig. 3. TEM images of the SACNT/ Mn_3O_4 composites obtained by decomposition of a) 3 wt%, b) 5 wt%, and c) 10 wt% $\text{Mn}(\text{NO}_3)_2$ solution infiltrated in SACNT film, containing a) 29 wt%, b) 47 wt%, and c) 78 wt% Mn_3O_4 , d)–f) present different size distributions of the Mn_3O_4 particles in the $\text{Mn}_3\text{O}_4/\text{SACNT}$ samples.

composites were $1121.5 \text{ mAh g}^{-1}$ and $1108.4 \text{ mAh g}^{-1}$, respectively (see in Fig. 5b). During cycling, the specific capacity gradually increased, with the highest capacity even reaching 1600 mAh g^{-1} and 1300 mAh g^{-1} for the 29 wt% and 47 wt% $\text{Mn}_3\text{O}_4/\text{SACNT}$ composites. Similar phenomena of capacity increase upon cycling have been observed in many nanostructured transition metal oxides [26,32,33], and the mechanism might be related to the formation of the SEI film/surface polymer (gel-like) coating or the formation of high oxidation state products [28,32].

To further explore the different electrochemical properties of the 29 wt%, 47 wt%, and 78 wt% $\text{Mn}_3\text{O}_4/\text{SACNT}$ composites, their discharge curves of the 1st, 2nd, and 40th cycles were compared. As shown in Fig. 6, the discharge curves at the 1st and 2nd cycles all shared common characteristics: 1) A sloped region above the plateau of 0.4–0.5 V, which may result from the formation of solid

electrolyte interface (SEI) film and the reduction of Mn_3O_4 to Mn (II) [34]. 2) A plateau at 0.4 V at the 1st cycle, which increased to 0.5 V at the 2nd cycle. This plateau corresponded to further reduction of Mn (II) to Mn (0) [34]. The voltage difference of the plateau between the 1st and 2nd cycles is mainly related to the large surface area and amorphization effect [35,36]. 3) A sloped region below the plateau, which was probably caused by an interfacial charging mechanism [27]. The 29 wt%, 47 wt%, and 78 wt% $\text{Mn}_3\text{O}_4/\text{SACNT}$ composites displayed different discharge curves at the 40th cycle. The discharge curves of both the 29 wt% and 47 wt% $\text{Mn}_3\text{O}_4/\text{SACNT}$ composites kept the original shape, with the plateau becoming a little sloped. This sloping is consistent with the smoother anodic peak around 0.4 V in the cyclic voltammetry curve at the 40th cycle (Fig. S1). While for the 78 wt% $\text{Mn}_3\text{O}_4/\text{SACNT}$ composite, the plateau of the discharge curve at the 40th cycle decreased to 0.2 V,

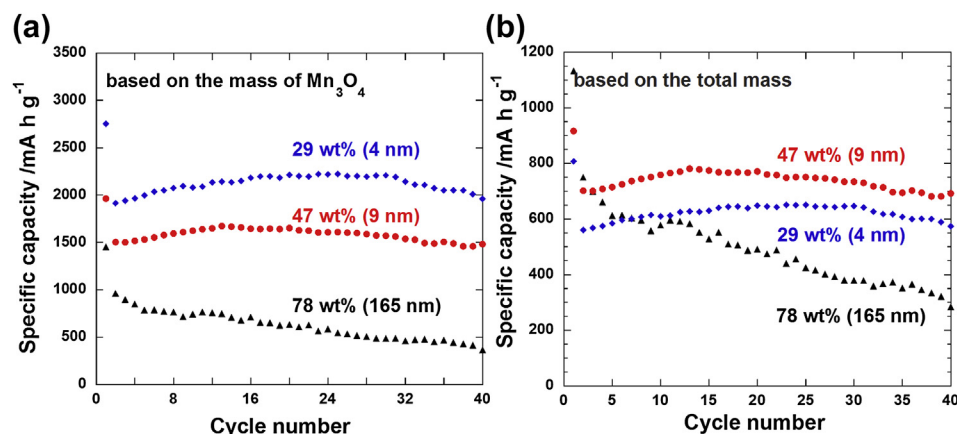


Fig. 4. Cycle performance of the $\text{Mn}_3\text{O}_4/\text{SACNT}$ films based on the mass of a) Mn_3O_4 , and b) electrodes (including Mn_3O_4 and SACNT).

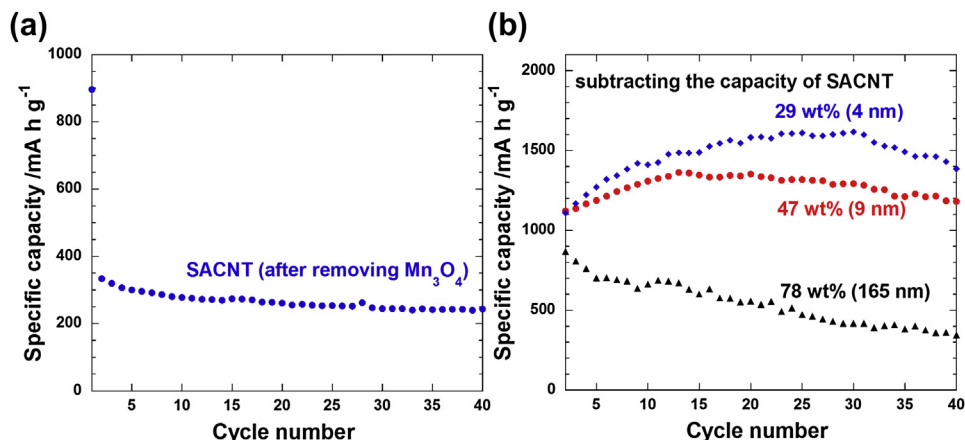


Fig. 5. a) Cycle performance of the SACNT film after dissolving Mn_3O_4 in hydrochloric acid. b) The capacity of Mn_3O_4 in the $\text{Mn}_3\text{O}_4/\text{SACNT}$ films after subtracting the capacity contribution of SACNT (derived from Figs. 4a and 5a).

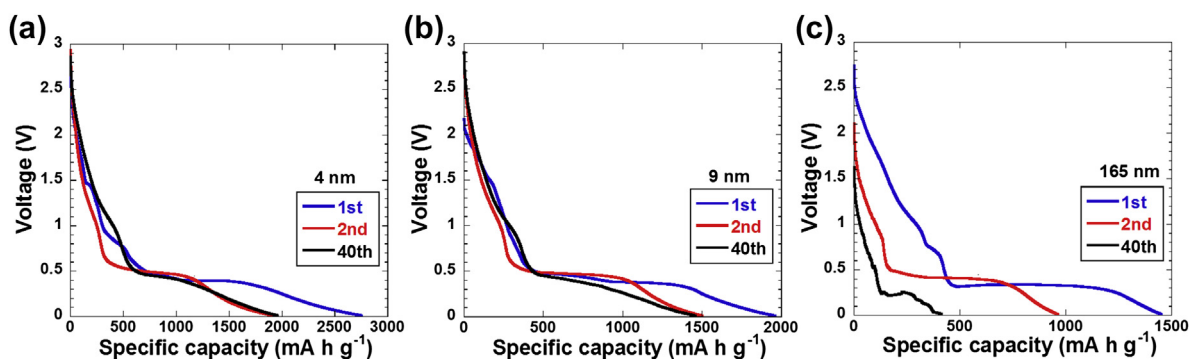


Fig. 6. Discharge curves of a) 29 wt%, b) 47 wt%, and c) 78 wt% $\text{Mn}_3\text{O}_4/\text{SACNT}$ composites, at the 1st, 2nd, and 40th cycles.

indicating further polarization at the 40th cycle than the 1st and 2nd cycles. The increase in the extent of polarization was often associated with severe agglomeration, low conductivity, or structural instability. In the 78 wt% $\text{Mn}_3\text{O}_4/\text{SACNT}$ electrode, the primary Mn_3O_4 particles agglomerated into secondary particles with a large size of 165 nm, therefore electron transfer among the Mn_3O_4 particles and SACNTs became less efficient, resulting in severe polarization and rapid capacity fading during cycling. On the contrary, the excellent reversibility in the discharge curves of the 29 wt% and 47 wt% $\text{Mn}_3\text{O}_4/\text{SACNT}$ electrodes is associated with homogeneous dispersion of Mn_3O_4 nanoparticles (less than 10 nm) anchored on the conductive SACNT films and the improved structural stability of the composites.

The voltage hysteresis (ΔU), corresponding to the difference between the charge and discharge voltages of the same lithiated state (Fig. 7a), was also compared among the 29 wt%, 47 wt%, and 78 wt% $\text{Mn}_3\text{O}_4/\text{SACNT}$ composites to demonstrate their difference in the extent of polarization. As shown in Fig. 7b and c (calculated from Fig. S2), the 78 wt% $\text{Mn}_3\text{O}_4/\text{SACNT}$ electrode with larger Mn_3O_4 particles (165 nm) had higher ΔU than the 47 wt% and 29 wt% $\text{Mn}_3\text{O}_4/\text{SACNT}$ electrodes with smaller Mn_3O_4 particles (9 nm and 4 nm). ΔU curve of the 29 wt% $\text{Mn}_3\text{O}_4/\text{SACNT}$ is not shown here, as the 29 wt% and 47 wt% $\text{Mn}_3\text{O}_4/\text{SACNT}$ composites shared the same characteristic of the ΔU curves (Figs. S2a and S2b). Another important aspect is that the increase in ΔU was around 0.4–0.5 V after 40 cycles for the 78 wt% $\text{Mn}_3\text{O}_4/\text{SACNT}$ electrode. While for

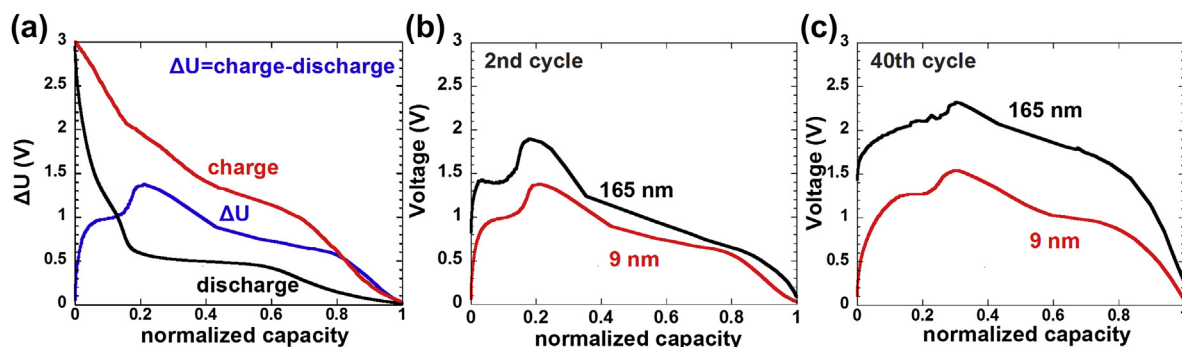


Fig. 7. a) Illustration of the calculation of voltage hysteresis (ΔU). ΔU for the b) 2nd and c) 40th cycles of the 47 wt% and 78 wt% $\text{Mn}_3\text{O}_4/\text{SACNT}$ composites.

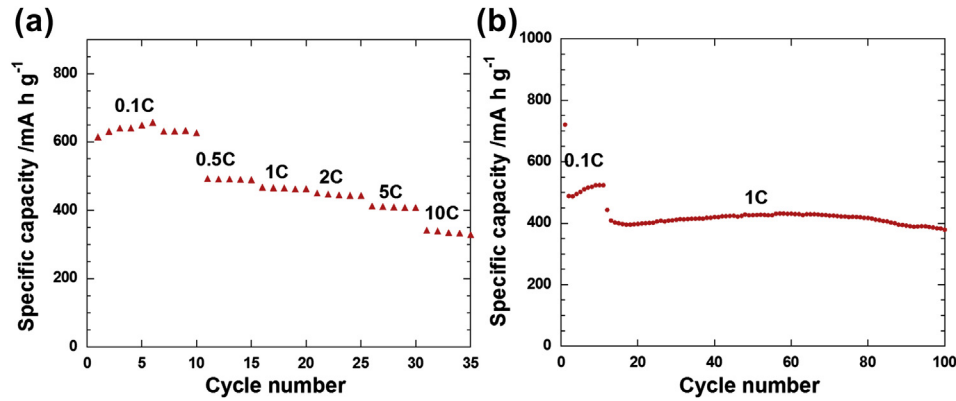


Fig. 8. Outstanding electrochemical performance of the nano-sized Mn₃O₄ particles (<10 nm) anchored on the SACNT films: a) rate capability and b) cycle performance at 1 C.

the 47 wt% and 29 wt% Mn₃O₄/SACNT electrodes, the increase in ΔU was only 0.1 V after 40 cycles, which further confirmed their better cycling stability than the 78 wt% Mn₃O₄/SACNT composite. Our experimental results suggest that nano-sized Mn₃O₄ (less than 10 nm) anchored on the SACNT films would present less extent of polarization and better reversibility than the agglomerated large Mn₃O₄ particles. Such size effect on the electrochemical performance in other transition metal oxides was also reported in literature [37].

With the Mn₃O₄ nanoparticles less than 10 nm, the Mn₃O₄/SACNT composite displayed excellent rate performance. As shown in Fig. 8a, a high capacity of 342 mA h g⁻¹ (based on the total mass of the electrode) at 10 C was obtained, corresponding to a retention of 53% compared to the capacity of 650 mA h g⁻¹ at 0.1 C. The cycling performance at high rate is also appealing. As presented in Fig. 8b, the capacity retention of the Mn₃O₄/SACNT composite still remained at 95% after 100 cycles at 1 C. To our knowledge, this result is outstanding among the published data of Mn₃O₄ nanocomposites. Particularly, these Mn₃O₄/SACNT composite electrodes do not require additional binder, conductive agent, or current

collector, which are beneficial for increasing the gravimetric and volumetric energy densities of the electrodes. The excellent electrochemical performance of the Mn₃O₄/SACNT composite with the Mn₃O₄ nanoparticles less than 10 nm is ascribed to the following aspects: 1) The cross-stacked SACNT film acted as the conductive network connecting all the Mn₃O₄ nanoparticles on it. The porous structure of the composite film also helped to accommodate the volume change and prevent agglomeration during cycling. 2) The nanosized Mn₃O₄ particles (<10 nm) anchored on the SACNT films have large specific reactive surface area and short diffusion distance, which benefit the rapid ion migration and fast reaction rate. Moreover, the excessive capacity shows pseudocapacitive character as suggested in Tarascon's surface polymer/gel-like coating model [28], and this part of capacity should maintain large at high rate.

The specific capacities of the Mn₃O₄/SACNT composites and the commercial graphite at different rates were also compared (Fig. 9). The capacity of graphite was calculated in two ways, with one based on the mass of graphite alone and the other based on the total mass of the electrode (including the conductive agent, binder, and current collector). The capacities based on the mass of graphite alone were 333 mA h g⁻¹ at 0.1 C and 276 mA h g⁻¹ at 2 C. While the capacities of Mn₃O₄/SACNT were 650 mA h g⁻¹ at 0.1 C and 449 mA h g⁻¹ at 2 C, 2 times and 1.6 times those of graphite alone respectively. When the masses of the conductive agent (5 wt%), binder (5 wt%), and current collector (10 μ m thick copper, about half of the electrode mass) in the graphite electrode were also considered, the superiority of the Mn₃O₄/SACNT (without any binder or current collector) became more obvious, 5 times at 0.1 C and 4.3 times at 2 C the capacity of the graphite electrode. This outstanding performance of the Mn₃O₄/SACNT composites over the commercial graphite indicates their potential in practical applications.

4. Conclusion

In conclusion, we prepared nano-Mn₃O₄/SACNT electrodes with a fine structure of Mn₃O₄ nanoparticles anchored on the cross-stacked SACNT scaffold, which showed stable cycling capability and excellent rate performance. In the Mn₃O₄/SACNT composite, SACNT films act as both conductive pathway and structural scaffold, so that no binder or current collector is needed. The particle size of Mn₃O₄ in the Mn₃O₄/SACNT composites was also tuned. It was found that the Mn₃O₄/SACNT composites with size of Mn₃O₄ less than 10 nm demonstrated higher capacity, less extent of polarization, and better cycle stability than the Mn₃O₄/SACNT composite with size of Mn₃O₄ at 165 nm. The optimized Mn₃O₄/SACNT composite displayed a capacity of more than 700 mA h g⁻¹ at 0.1 C (based on the total mass of the electrode). A large capacity of

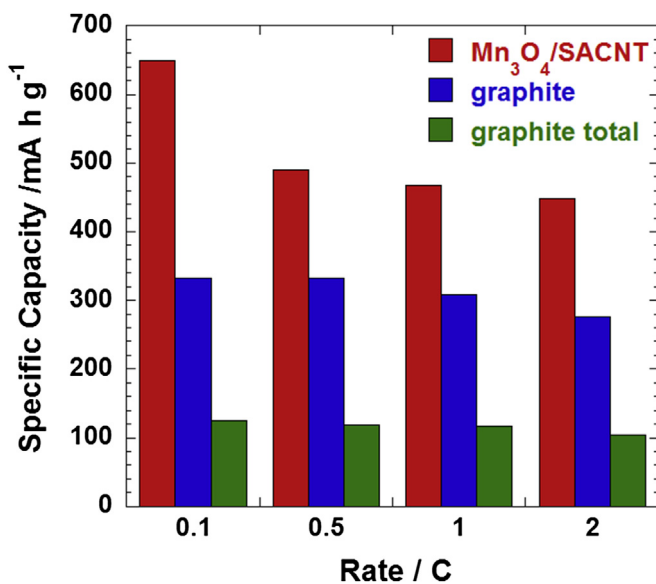


Fig. 9. Comparison of the rate capacities among Mn₃O₄/SACNT electrode (based on the total mass of Mn₃O₄ and SACNT), graphite active material (based on the mass of graphite alone), and graphite electrode (based on the total mass of graphite, conducting agent, binder, and current collector).

342 mAh g⁻¹ can still be obtained at a high rate of 10 C, and a capacity retention of 95% was achieved for 100 cycles at 1 C. This superior electrochemical performance including stable cycling stability and excellent rate performance demonstrates the advantages of the Mn₃O₄/SACNT composites over the commercial graphite anode and their potential applications in LIBs.

Acknowledgments

This work was supported by the National Basic Research Program of China (2012CB932301) and the NSFC (51102146).

Appendix A. Supplementary data

Supplementary data related to this article can be found at <http://dx.doi.org/10.1016/j.jpowsour.2013.10.133>.

References

- [1] P. Poizot, S. Laruelle, S. Grugeon, L. Dupont, J.M. Tarascon, *Nature* 407 (2000) 496–499.
- [2] P.G. Bruce, B. Scrosati, J.M. Tarascon, *Angew. Chem. Int. Ed.* 47 (2008) 2930–2946.
- [3] H. Li, G. Richter, J. Maier, *Adv. Mater.* 15 (2003) 736–739.
- [4] P. Balaya, H. Li, L. Kienle, J. Maier, *Adv. Funct. Mater.* 13 (2003) 621–625.
- [5] S. Grugeon, S. Laruelle, R. Herrera-Urbina, L. Dupont, P. Poizot, J.M. Tarascon, *J. Electrochem. Soc.* 148 (2001) A285–A292.
- [6] J. Cabana, L. Monconduit, D. Larcher, M.R. Palacin, *Adv. Mater.* 22 (2010) E170–E192.
- [7] A.S. Arico, P. Bruce, B. Scrosati, J.M. Tarascon, W. Van Schalkwijk, *Nat. Mater.* 4 (2005) 366–377.
- [8] C. Chae, J.H. Kim, J.M. Kim, Y. Sun, J.K. Lee, *J. Mater. Chem.* 22 (2012) 17870–17877.
- [9] K.F. Zhong, B. Zhang, S.H. Luo, W. Wen, H. Li, X.J. Huang, L.Q. Chen, *J. Power Sources* 196 (2011) 6802–6808.
- [10] H.L. Wang, L.F. Cui, Y.A. Yang, H.S. Casalongue, J.T. Robinson, Y.Y. Liang, Y. Cui, H.J. Dai, *J. Am. Chem. Soc.* 132 (2010) 13978–13980.
- [11] D. Pasero, N. Reeves, A.R. West, *J. Power Sources* 141 (2005) 156–158.
- [12] D.P. Dubal, R. Holze, *RSC Adv.* 2 (2012) 12096–12100.
- [13] J. Gao, M.A. Lowe, H.D. Abruna, *Chem. Mater.* 23 (2011) 3223–3227.
- [14] J.Z. Wang, N. Du, H. Wu, H. Zhang, J.X. Yu, D.R. Yang, *J. Power Sources* 222 (2013) 32–37.
- [15] N. Lavoie, P. Malenfant, F.M. Courtel, Y. Abu-Lebdeh, I.J. Davidson, *J. Power Sources* 213 (2012) 249–254.
- [16] Z.H. Wang, L.X. Yuan, Q.G. Shao, F. Huang, Y.H. Huang, *Mater. Lett.* 80 (2012) 110–113.
- [17] L. Li, Z.P. Guo, A.J. Du, H.K. Liu, *J. Mater. Chem.* 22 (2012) 3600–3605.
- [18] J. Guo, Q. Liu, C. Wang, M.R. Zachariah, *Adv. Funct. Mater.* 22 (2012) 803–811.
- [19] K.L. Jiang, Q.Q. Li, S.S. Fan, *Nature* 419 (2002) 801.
- [20] K.L. Jiang, J.P. Wang, Q.Q. Li, L.A. Liu, C.H. Liu, S.S. Fan, *Adv. Mater.* 23 (2011) 1154–1161.
- [21] S. Luo, K. Wang, J. Wang, K. Jiang, Q. Li, S. Fan, *Adv. Mater.* 24 (2012) 2294–2298.
- [22] K. Wang, S. Luo, Y. Wu, X. He, F. Zhao, J. Wang, K. Jiang, S. Fan, *Adv. Funct. Mater.* 23 (2013) 846–853.
- [23] Y. Wu, Y. Wei, J. Wang, K. Jiang, S. Fan, *Nano Lett.* 13 (2013) 818–823.
- [24] H.X. Zhang, C. Feng, Y.C. Zhai, K.L. Jiang, Q.Q. Li, S.S. Fan, *Adv. Mater.* 21 (2009) 2299.
- [25] X.B. Zhang, K.L. Jiang, C. Teng, P. Liu, L. Zhang, J. Kong, T.H. Zhang, Q.Q. Li, S.S. Fan, *Adv. Mater.* 18 (2006) 1505.
- [26] Y.M. Sun, X.L. Hu, W. Luo, F.F. Xia, Y.H. Huang, *Adv. Funct. Mater.* 23 (2013) 2436–2444.
- [27] J. Jamnik, J. Maier, *Phys. Chem. Chem. Phys.* 5 (2003) 5215–5220.
- [28] S. Laruelle, S. Grugeon, P. Poizot, M. Dolle, L. Dupont, J.M. Tarascon, *J. Electrochem. Soc.* 149 (2002) A627–A634.
- [29] V. Meunier, J. Kephart, C. Roland, J. Bernholc, *Phys. Rev. Lett.* 88 (2002).
- [30] B.J. Landi, M.J. Ganter, C.D. Cress, R.A. DiLeo, R.P. Raffaele, *Energy Environ. Sci.* 2 (2009) 638–654.
- [31] V. Datsyuk, M. Kalyva, K. Papagelis, J. Parthenios, D. Tasis, A. Siokou, I. Kallitsis, C. Galiotis, *Carbon* 46 (2008) 833–840.
- [32] C.M. Ban, Z.C. Wu, D.T. Gillaspie, L. Chen, Y.F. Yan, J.L. Blackburn, A.C. Dillon, *Adv. Mater.* 22 (2010) E145.
- [33] K. Zhong, X. Xia, B. Zhang, H. Li, Z. Wang, L. Chen, *J. Power Sources* 195 (2010) 3300–3308.
- [34] X.P. Fang, X. Lu, X.W. Guo, Y. Mao, Y.S. Hu, J.Z. Wang, Z.X. Wang, F. Wu, H.K. Liu, L.Q. Chen, *Electrochem. Commun.* 12 (2010) 1520–1523.
- [35] Y.J. Mai, D. Zhang, Y.Q. Qiao, C.D. Gu, X.L. Wang, J.P. Tu, *J. Power Sources* 216 (2012) 201–207.
- [36] H. Li, P. Balaya, J. Maier, *J. Electrochem. Soc.* 151 (2004) A1878–A1885.
- [37] D. Larcher, C. Masquelier, D. Bonnin, Y. Chabre, V. Masson, J.B. Leriche, J.M. Tarascon, *J. Electrochem. Soc.* 150 (2003) A133–A139.